SCIENCE CHINA
Physics, Mechanics & Astronomy

• Article •
Editor's Focus

March 2021 Vol. 64 No. 3: 234262
https://doi.org/10.1007/s11433-020-1625-9

Editor's Focus

On-chip erbium-doped lithium niobate microcavity laser

YiAn Liu†, XiongShuo Yan†, JiangWei Wu, Bing Zhu, YuPing Chen*, and XianFeng Chen*

State Key Laboratory of Advanced Optical Communication Systems and Networks, School of Physics and Astronomy, Shanghai Jiao Tong University, Shanghai 200240, China

Received September 28, 2020; accepted October 4, 2020; published online October 30, 2020

The commercialization of lithium niobate on insulator (LNOI) wafer has resulted in significant on-chip photonic integration application owing to its remarkable photonic, acousto-optic, electro-optic, and piezoelectric nature. In recent years, a variety of high-performance on-chip LNOI-based photonic devices have been realized. In this study, we developed a 1-mol% erbium-doped lithium niobate crystal and its LNOI on a silicon substrate and fabricated an erbium-doped LNOI microdisk with high quality factor (~ 1.05×10^5). C-band laser emission at ~1530 and ~1560 nm (linewidth 0.12 nm) from the high-Q erbium-doped LNOI microdisk was demonstrated with 974- and 1460-nm pumping, with the latter having better thermal stability. This microlaser would play an important role in the photonic integrated circuits of the lithium niobate platform.

erbium-doped lithium niobate on insulator, on-chip laser, microdisk

PACS number(s): 42.82.-m, 42.60.Da, 42.70.Mp, 42.55.-f

Citation: Y. A. Liu, X. S. Yan, J. W. Wu, B. Zhu, Y. P. Chen, and X. F. Chen, On-chip erbium-doped lithium niobate microcavity laser, Sci. China-Phys. Mech. Astron. **64**, 234262 (2021), https://doi.org/10.1007/s11433-020-1625-9

1 Introduction

Lithium niobate on insulator (LNOI) has been a research hotspot in recent years. Owing to the excellent physical properties of lithium niobate (e.g., nonlinearity, electro-optic, acousto-optic, and piezoelectric effects), many on-chip devices have been developed, such as a frequency doubler, modulator, and filter [1-10]. To realize the complete photonic integrated circuits (PICs) on lithium niobate (LN) chips and meet the requirements of future high-speed optical communications, a C-band light source on LN chips urgently needs to be developed. It is known that rare earth erbium ion doping can produce lasers in the C-band, and many types of Er^{3+}-doped lasers based on waveguides have been developed [11, 12]. However, these Er^{3+}-doped lasers are difficult to integrate on-chip. Considering that the on-chip laser requires a small footprint for PICs, a high-quality-factor whispering gallery mode microdisk or microring resonator lasers are a good choice [13-19]. Therefore, an erbium-doped microdisk laser on an LN chip may benefit the research on PICs. Notably, Er^{3+} doping of LNOI by ion implantation has been achieved in a previous study; however, owing to the low doping concentration and nonuniform distribution of Er^{3+}, the device does not exhibit good laser output characteristics [20]. Herein, we directly grew the erbium-doped LN crystal and transformed it into an LNOI wafer. Then, a 150-μm-diameter microdisk cavity was fabricated on Er^{3+}-doped 600-nm-thick z-cut LNOI, and the C-band laser output from the microdisk was observed. The laser thresholds of 974- and 1460-nm pumps were 2.99 and 9.31 mW, respectively. The LNOI light source is a big step forward in the development of LN PICs.

*Corresponding authors (YuPing Chen, email: ypchen@sjtu.edu.cn; XianFeng Chen, email: xfchen@sjtu.edu.cn)
† These authors contributed equally to this work.

2 Fabrication

1% mol Er^{3+} ion is doped into LN during the crystal growth process, as shown in Figure 1(a). The Er^{3+}-doped 600-nm-thick z-cut LNOI, with 2-μm silica and 400-μm silicon substrate, is fabricated by the smart-cut method from a 3-inch wafer [21], as shown in Figure 1(b)-(d). The microdisk with a 150-μm-diameter was fabricated by focused ion beam (FIB) milling (ZEISS Auriga), as shown in Figure 1(f). After FIB milling, a microring scanning pattern was used to remove residue at the edge of the microdisk, which allows to obtain a smooth sidewall and achieve high optical Q factor. Then, the sample was immersed in a buffered oxide etching (BOE) solution to form a silica pedestal under the Er^{3+}-doped LNOI microdisk, as shown in Figure 1(g) and (h). Typically, a silica pedestal has a nearly round border after BOE owing to the isotropic corrosion of silica. However, in our device, we observed that the silica pedestal was not a regular circle. This occurred because silicon dioxide in the intermediate layer is not uniformly bonded to Er^{3+}-doped LN. Moreover, further steps (e.g., chemo-mechanical polishing) can help achieve a higher Q factor [22-24] owing to the smoother surface morphology.

3 Results and discussion

Figure 2(a) shows the experimental setup. First, the Q factor of the Er^{3+}-doped LNOI microdisk was characterized using a C-band tunable continuous-wave laser (New Focus TLB-6728, linewidth < 200 kHz, 1520-1570 nm). A polarization controller was used to control the polarization of the input light. The tapered fiber, which was made using the heating and pulling method, was used to couple light into and out of the Er^{3+}-doped LNOI microdisk. The waist diameter of the tapered fiber was approximately ~1 μm.

The Er^{3+}-doped LNOI microdisk was placed on a precision 3D nanostage, which was positioned under an optical microscope. Thus, we could readily adjust the contact point and distance between the tapered fiber and the Er^{3+}-doped LNOI microdisk to optimize the coupling efficiency or controlling the lasing wavelength [13]. Then, the transmitted light from the tapered fiber was linked to an InGaAs photodetector (PD) and an oscilloscope (OSC) to monitor the transmission spectrum.

We scanned the C-band laser wavelength from 1550 to 1560 nm under loading with a relatively low optical power, which was sufficient for measuring the transmission spectrum of the microdisk, to avoid interference from thermal effects. The transmission spectrum of the microdisk is shown in Figure 2(b). The Q factor of the mode indicated by a dotted black frame in Figure 2(b) was measured to be 1.05×10^5, shown in Figure 2(c), which was slightly lower than our previous microdisk resonator [25] owing to the absorption of doped Er^{3+}. Then, we used 974- and 1460-nm LD light sources (Golight Co., Ltd) to achieve efficient laser emission in the Er^{3+}-doped LNOI microdisk, as shown in Figure 2(a). The strong green emission was observed by a CCD camera, as shown in the inset in Figure 3(a).

The spectrum was measured by an optical spectrum analyzer (200-1100 nm) under 974-nm pump, as shown in Figure 3(a). Notably, the spectrum under 1460-nm pump is similar to that under the 974 nm pump. Green and red emissions are produced by the cooperation up-conversion (CUC) and excited-state absorption (ESA) of the 974-nm pump, respectively, as shown in Figure 3(b) (i). Figure 3(b) (ii) shows that the second-order CUC of the 1460-nm pump generates green

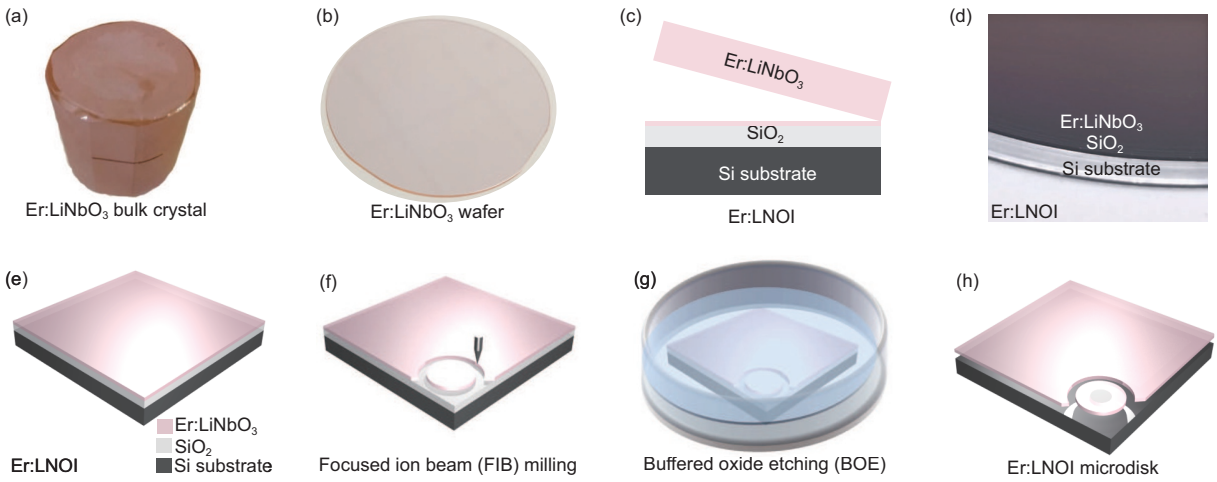

Figure 1 (Color online) (a)-(d) Er^{3+}-doped LNOI fabrication process, where (a), (b), and (d) are images of real samples. (e)-(h) Microdisk fabrication process.

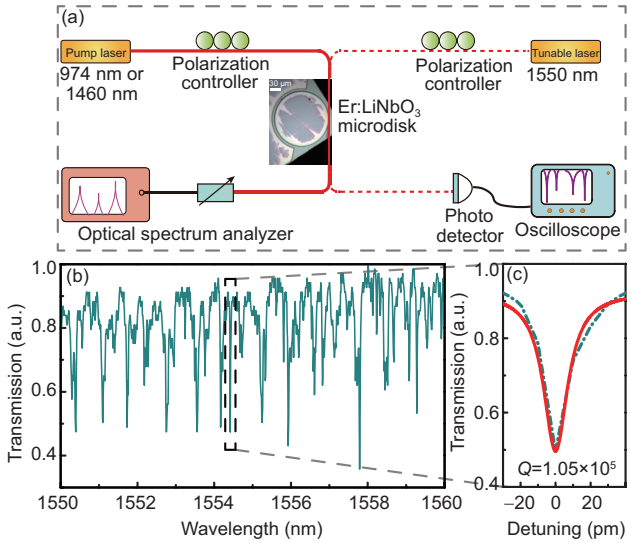

Figure 2 (Color online) (a) Schematic of the experimental setup; (b) transmission spectrum of the 150-μm-diameter Z-cut Er^{3+}-doped LNOI microdisk from 1550 to 1560 nm; (c) Lorentzian fitting of a measured mode around 1554.42 nm indicated by a dotted black frame in (b), exhibiting a Q factor of 1.05×10^5.

and red emissions [26].

The Er^{3+}-doped LNOI microdisk laser spectrum was measured with optical spectrum analyzer (0.6-1.75 μm). Figure 4(a) shows the laser spectrum at the C-band, pumped by a 974-nm laser. The observed linewidth was 0.12 nm, as shown in Figure 4(b) and (c). The laser output power at 1531.6 nm was recorded versus the pump power. The threshold and slope efficiency were calculated to be 2.99 mW and 4.117×10^{-6}, respectively, as shown in Figure 4(d). The laser spectrum at the C-band, pumped by a 1460-nm laser, was also measured, as shown in Figure 4(e); the calculated threshold and slope efficiency of the 1531.6-nm laser were 9.31 mW and 3.15×10^{-5}, as shown in Figure 4(h), respectively. The observed linewidth was 0.14 nm, as shown in Figure 4(f) and (g). As shown in Figure 4(e), laser emission is considerably different when the pump power is changed. This can be explained by the mode competition in inhomogeneous broad lasers. Owing to the small frequency distance between adjacent resonance modes in this relatively large multimode microdisk, mode competition appears with an increase in the pump power, which leads to the change in laser wavelength [27]. Note that the laser slope efficiency under the 1460-nm pump is higher than that under the 974-nm pump, which may be caused by the different coupling efficiencies of the two pump lasers. We may introduce chaos into the microdisk to improve the coupling efficiency of the 1460-nm pump [18].

When measuring the threshold, we determined that the laser wavelength drifts with a change in the pump power. For the convenience and accuracy of the experiment, we chose a laser wavelength of approximately 1560 nm. With the pump at 974 nm, a single laser emission at approximately 1560 nm exhibited a red-shift with an increase in the pump power, as shown in Figure 5(a). The laser wavelength linearly drifted with the pump power at the slope of 47.9 pm/mW, as shown in Figure 5(b). The red-shift arises from the temperature increase in the microdisk, which is related to the pump laser. An extra temperature-control device may reduce the red-shift.

With 1460-nm laser pumping, the laser emission wavelength at approximately 1561-nm exhibited a drift, as shown in Figure 5(c). The linear wavelength drift with the pump power was also calculated at the slope of 22.5 pm/mW, as shown in Figure 5(d). By comparing the wavelength drift slope, we observed that pumping with a 1460-nm laser provided better thermal stability. This occurred because the 974-nm pump laser included an ESA process that could store

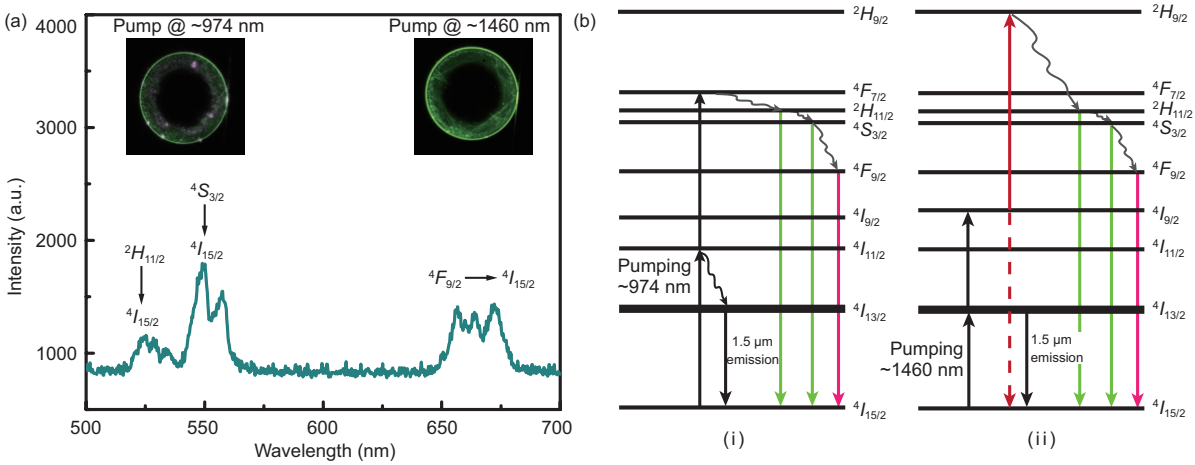

Figure 3 (Color online) (a) Visible emission spectrum at 974-nm pumping of the Er^{3+}-doped LNOI microdisk. The two insets show the optical microscope images of visible emission from the Er^{3+}-doped LNOI microdisk, with 974- and 1460-nm laser pumping, respectively. (b) Energy levels of Er^{3+} involved in up-conversion emission. (i) First-order CUC and ESA; (ii) second-order CUC.

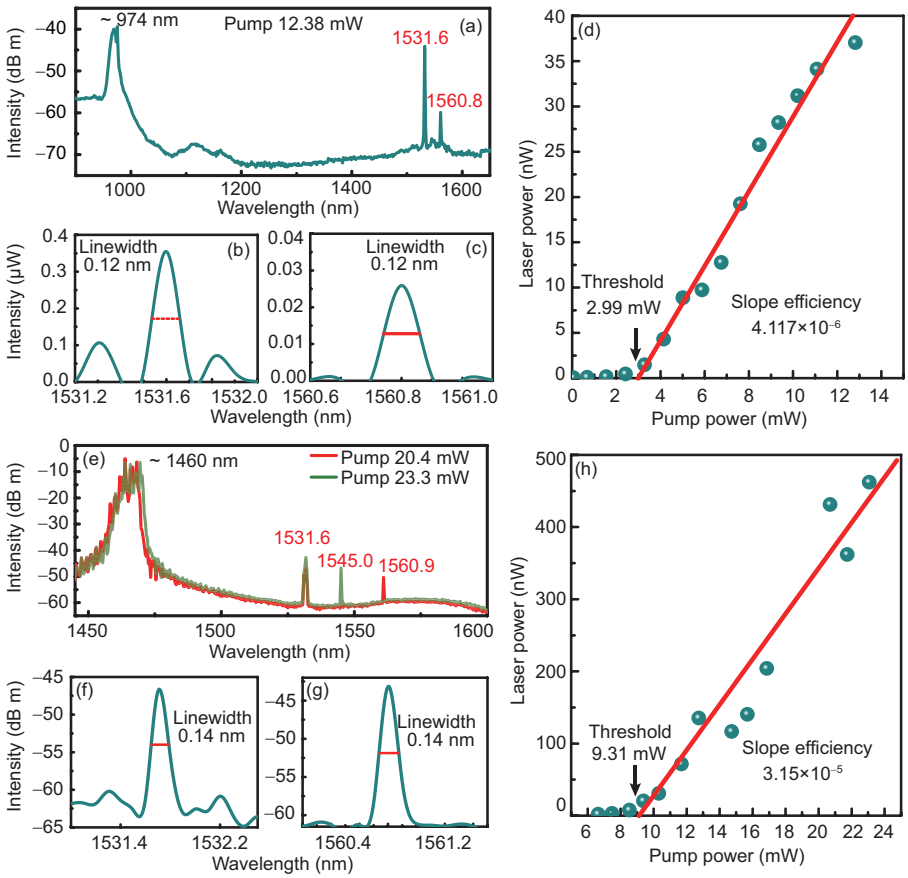

Figure 4 (Color online) Er^{3+}-doped LNOI microdisk laser spectrum and threshold characteristics. (a) Observed laser spectrum with the 974-nm pump; (b), (c) laser linewidth with the 974-nm pump; (d) relationship between emitted laser power and the 974-nm pump power; (e) observed laser spectrum with the 1460-nm pump at different pump powers; (f), (g) laser linewidth with the 1460-nm pump; (h) relationship between the emitted laser power and the 1460-nm pump power.

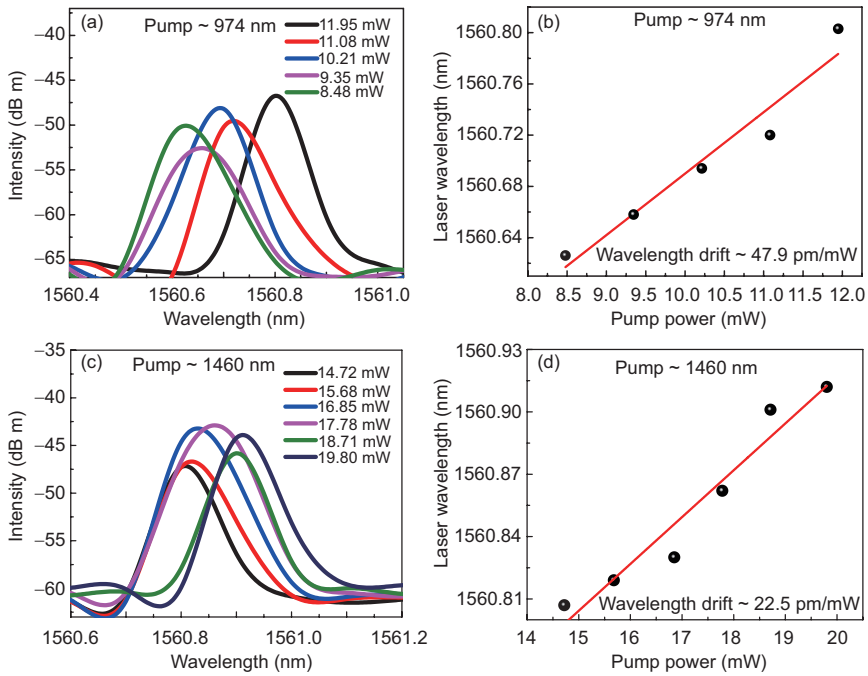

Figure 5 (Color online) Laser wavelength drift with different pump powers. (a), (c) Measured laser wavelength with different pump power; (b), (d) linear fit of the laser wavelength drift.

more pump laser energy in the microdisk. However, this phenomenon requires further study.

4 Conclusions

In summary, a high-Q Er^{3+}-doped LNOI microdisk was fabricated. By pumping with 974-nm and 1460-nm lasers, both visible and C-band laser emissions were observed. The C-band laser threshold with the 974-nm and 1460-nm pumps was 2.99 and 9.31 mW, respectively. The laser wavelength drift with a change in the power of the 974- and 1460-nm pumps was also calculated and analyzed. Combining the properties of doping erbium with the excellent nonlinear, electro-optic, acousto-optic, and integrated properties of LNOI, the development of many classes of new and higher functional devices can be expected in PICs such as on-chip LN amplifier and tunable laser.

This work was supported by the National Key R&D Program of China (Grant Nos. 2019YFB2203500, and 2017YFA0303700), the National Natural Science Foundation of China (Grant No. 91950107), and the Foundation for Development of Science and Technology of Shanghai (Grant No. 17JC1400400). We would like to acknowledge Shanghai Daheng Optics and Fine Mechanics Co., Ltd. and Jinan Jingzheng Electronics Co., Ltd. for the Er^{3+}-doped LNOI cooperative research and development. We also acknowledge the Center for Advanced Electronic Materials and Devices (AEMD) of Shanghai Jiao Tong University for the microdisk fabrication.

1 C. Wang, M. Zhang, X. Chen, M. Bertrand, A. Shams-Ansari, S. Chandrasekhar, P. Winzer, and M. Lončar, Nature **562**, 101 (2018).
2 M. Li, J. Ling, Y. He, U. A. Javid, S. Xue, and Q. Lin, Nat. Commun. **11**, 4123 (2020), arXiv: 2003.03259.
3 L. Shao, M. Yu, S. Maity, N. Sinclair, L. Zheng, C. Chia, A. Shams-Ansari, C. Wang, M. Zhang, K. Lai, and M. Lončar, Optica **6**, 1498 (2019), arXiv: 1907.08593.
4 L. Ge, Y. Chen, H. Jiang, G. Li, B. Zhu, Y. Liu, and X. Chen, Photon. Res. **6**, 954 (2018).
5 J. Lin, N. Yao, Z. Hao, J. Zhang, W. Mao, M. Wang, W. Chu, R. Wu, Z. Fang, L. Qiao, W. Fang, F. Bo, and Y. Cheng, Phys. Rev. Lett. **122**, 173903 (2019).
6 A. Boes, B. Corcoran, L. Chang, J. Bowers, and A. Mitchell, Laser Photon. Rev. **12**, 1700256 (2018).
7 S. Mossman, and M. G. Kuzyk, Opt. Lett. **44**, 5 (2019), arXiv: 1809.01216.
8 H. Jiang, X. Yan, H. Liang, R. Luo, X. Chen, Y. Chen, and Q. Lin, Appl. Phys. Lett. **117**, 081102 (2020).
9 M. He, M. Xu, Y. Ren, J. Jian, Z. Ruan, Y. Xu, S. Gao, S. Sun, X. Wen, L. Zhou, L. Liu, C. Guo, H. Chen, S. Yu, L. Liu, and X. Cai, Nat. Photonics **13**, 359 (2019), arXiv: 1807.10362.
10 Z. Hao, L. Zhang, W. Mao, A. Gao, X. Gao, F. Gao, F. Bo, G. Zhang, and J. Xu, Photon. Res. **8**, 311 (2020).
11 S. V. Kravchenko, E. V. Byzov, M. A. Moiseev, and L. L. Doskolovich, Opt. Express **25**, A23 (2017).
12 W. Sohler, IEICE Trans. Electron. **E88-C**, 990 (2005).
13 B. Min, T. J. Kippenberg, L. Yang, K. J. Vahala, J. Kalkman, and A. Polman, Phys. Rev. A **70**, 033803 (2004).
14 L. Y. Karachinsky, S. Pellegrini, G. S. Buller, A. S. Shkolnik, N. Y. Gordeev, V. P. Evtikhiev, and V. B. Novikov, Appl. Phys. Lett. **84**, 7 (2004).
15 Y. Fang, A. Armin, P. Meredith, and J. Huang, Nat. Photonics **13**, 1 (2019).
16 Q. T. Cao, R. Liu, H. Wang, Y. K. Lu, C. W. Qiu, S. Rotter, Q. Gong, and Y. F. Xiao, Nat. Commun. **11**, 1136 (2020).
17 P. Latawiec, V. Venkataraman, M. J. Burek, B. J. M. Hausmann, I. Bulu, and M. Lončar, Optica **2**, 924 (2015), arXiv: 1509.00373.
18 X. Jiang, L. Shao, S. X. Zhang, X. Yi, J. Wiersig, L. Wang, Q. Gong, M. Lončar, L. Yang, and Y. F. Xiao, Science **358**, 344 (2017).
19 S. Zhu, L. Shi, B. Xiao, X. Zhang, and X. Fan, ACS Photonics **5**, 3794 (2018).
20 S. Wang, L. Yang, R. Cheng, Y. Xu, M. Shen, R. L. Cone, C. W. Thiel, and H. X. Tang, Appl. Phys. Lett. **116**, 151103 (2020), arXiv: 1912.07584.
21 G. Poberaj, H. Hu, W. Sohler, and P. Günter, Laser Photon. Rev. **6**, 488 (2012).
22 R. Wu, M. Wang, J. Xu, J. Qi, W. Chu, Z. Fang, J. Zhang, J. Zhou, L. Qiao, Z. Chai, J. Lin, and Y. Cheng, Nanomaterials **8**, 910 (2018).
23 J. Zhang, Z. Fang, J. Lin, J. Zhou, M. Wang, R. Wu, R. Gao, and Y. Cheng, Nanomaterials **9**, 1218 (2019).
24 M. Wang, R. Wu, J. Lin, J. Zhang, Z. Fang, Z. Chai, and Y. Cheng, Quantum Eng. **1**, e9 (2019).
25 L. Ge, H. Jiang, Y. Liu, B. Zhu, C. Lu, Y. Chen, and X. Chen, Opt. Mater. Express **9**, 1632 (2019), arXiv: 1809.06262.
26 V. Cappello, L. Marchetti, P. Parlanti, S. Landi, I. Tonazzini, M. Cecchini, V. Piazza, and M. Gemmi, Sci. Rep. **6**, 1 (2016).
27 B. K. Zhou, *Principles of Lasers* (National Defense Industry Press, Beijing, 2009), p. 167.